IOPscience iopscience.iop.org

Home Search Collections Journals About Contact us My IOPscience

Growth of graphene from SiC{0001} surfaces and its mechanisms

This content has been downloaded from IOPscience. Please scroll down to see the full text.

2014 Semicond. Sci. Technol. 29 064009

(http://iopscience.iop.org/0268-1242/29/6/064009)

View the table of contents for this issue, or go to the journal homepage for more

Download details:

IP Address: 129.120.87.225
This content was downloaded on 07/02/2017 at 17:15

Please note that terms and conditions apply.

You may also be interested in:

Structural features of epitaxial graphene on SiC {0001} surfaces
Wataru Norimatsu and Michiko Kusunoki

Combining graphene with silicon carbide: synthesis and properties – a review
Ivan Shtepliuk, Volodymyr Khranovskyy and Rositsa Yakimova

Growth and electronic transport properties of epitaxial graphene on SiC
H Hibino, S Tanabe, S Mizuno et al.

Epitaxial few-layer graphene: towards single crystal growth
H Hibino, H Kageshima and M Nagase

The growth and morphology of epitaxial multilayer graphene
J Hass, W A de Heer and E H Conrad

Epitaxial growth of boron-doped graphene by thermal decomposition of B4C
Wataru Norimatsu, Koichiro Hirata, Yuta Yamamoto et al.

The physics of epitaxial graphene on SiC(0001)
H Kageshima, H Hibino and S Tanabe

Low energy electron microscopy and photoemission electron microscopy investigation of graphene
K L Man and M S Altman

A critical review of growth of low-dimensional carbon nanostructures on SiC (0001): impact of growth environment
Weijie Lu, John J Boeckl and William C Mitchel

IOP Publishing Semiconductor Science and Technology
Semicond. Sci. Technol. 29 (2014) 064009 (11pp) doi:10.1088/0268-1242/29/6/064009

Growth of graphene from SiC{0001} surfaces and its mechanisms

Wataru Norimatsu[1] **and Michiko Kusunoki**[2]

[1] Department of Applied Chemistry, Graduate School of Engineering, Nagoya University, Furo-cho, Chikusa-ku, Nagoya-shi, Aichi-ken, 464-8603, Japan
[2] EcoTopia Science Institute, Nagoya University, Furo-cho, Chikusa-ku, Nagoya-shi, Aichi-ken, 464-8603, Japan

E-mail: w_norimatsu@esi.nagoya-u.ac.jp

Received 5 December 2013, revised 20 January 2014
Accepted for publication 23 January 2014
Published 6 May 2014

Abstract
Graphene, a one-atom-layer carbon material, can be grown by thermal decomposition of SiC. On Si-terminated SiC(0001), graphene nucleates at steps and grows layer-by-layer, and as a result a homogeneous monolayer or bilayer can be obtained. We demonstrate this mechanism both experimentally and theoretically. On the C-face $(000\bar{1})$, multilayer graphene nucleates not only at steps, but also on the terraces. These differences reflect the distinct differences in the reactivity of these faces. Due to its high quality and structural controllability, graphene on SiC{0001} surfaces will be a platform for high-speed graphene device applications.

Keywords: graphene, growth mechanism, silicon carbide

(Some figures may appear in colour only in the online journal)

1. Introduction

Layered materials have strong in-plane atomic and electronic interactions and weak out-of-plane interactions. These different interactions in the layered materials give rise to many surprising properties. The most familiar layered material is graphite, whose crystal and electronic structures have been investigated since the early 19th century [1, 2]. The in-plane and out-of-plane atomic bonds are covalent and van der Waals in nature, respectively. Its electronic structure is characterized by the slightly overlapping conduction and valence bands due to the interlayer interaction. Electrical and thermal transport strongly depends on its orientation; the in-plane electrical and thermal conductivity is about 10^5 and several hundred times, respectively, higher than the out-of-plane values [3, 4]. Another type of material, which has van der Waals interlayer interaction, are the layered chalcogenides. They include the tellurides and sulfides that are suitable for thermoelectric applications due to their excellent anisotropic electrical and thermal properties [5–10]. Yet other types of layered materials are layered oxides. Although some of them do not have the van der Waals interlayer interaction, many interesting properties have been discovered. The most striking is the occurrence of high-temperature superconductivity in the layered perovskite cuprates [11, 12]. This discovery produced an explosion in research into the charge, spin, orbital and lattice degrees of freedom in the MO_2 planes in the layered perovskite oxides, where M is the transition metal element, such as copper and manganese [13–16]. The commonality of the properties of the layered materials is the behavior of the electrical or thermal carrier confined in two dimensions.

In order to understand such two-dimensional properties, pure single-layer materials should be investigated. Novoselov and co-workers succeeded in exfoliating a single layer from single crystal graphite, transferring it onto a SiO_2/Si wafer, and revealing unusual phenomena that are characteristic of two-dimensional Dirac fermions [17, 18]. Graphene on a SiO_2/Si substrate absorbs visible light by 2.3%/monolayer, and so the number of layers can be identified under the optical microscope [17, 19]. Recently, new physics, including the anomalous quantum Hall effect have been observed in graphene deposited on hexagonal BN on a Si wafer, which indicates the presence of an ideally clean two-dimensional electron gas (2DEG) system [20, 21]. One of the most characteristic features of graphene is the linear band dispersion around the K point in reciprocal space [18]. Due to this feature, the electrons in graphene behave as massless Dirac fermions, and they have an extremely high carrier mobility [21].

 © 2014 IOP Publishing Ltd Printed in the UK

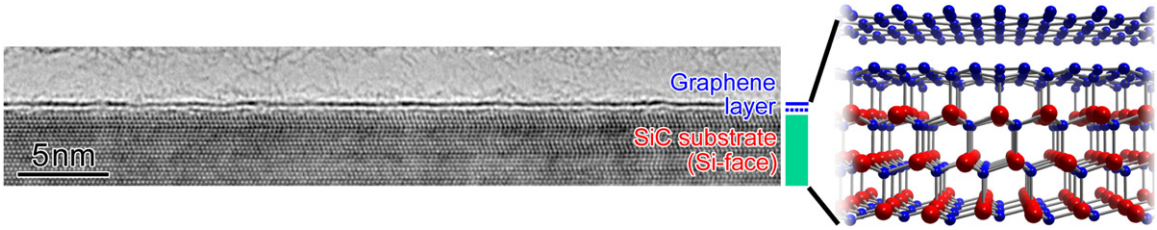

Figure 1. HRTEM image of monolayer graphene epitaxially grown on SiC{0001}. Red and blue spheres correspond to silicon and carbon atoms, respectively. The blue broken line (layer) corresponds to the buffer layer.

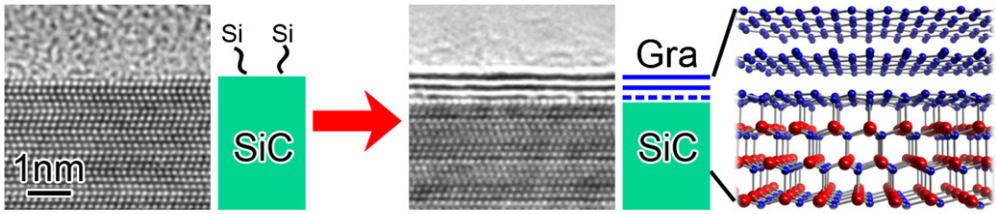

Figure 2. Basic phenomena of graphene growth by thermal decomposition of SiC.

A high carrier mobility should enable the development of high-speed electronics applications [22–24]. From the application point of view, the above mentioned mechanical exfoliation technique is not appropriate, because of the uncontrollable thickness, area and location. Large-area graphene growth is then necessary. For large-scale production, we have essentially two choices; chemical vapor deposition (CVD) and the thermal decomposition of SiC{0001} substrates.

In the CVD method, the vapor containing carbon is decomposed at a high temperature, and they form graphene on the catalytic metal substrate [25, 26]. Using a copper substrate, monolayer graphene can be easily obtained at low cost [26]. However, because of the use of the metal substrate, it is still necessary to transfer the graphene onto another insulating substrate for the electronics applications. It is widely known that the transfer process induces defects and impurities. In this sense, graphene growth by thermal decomposition of SiC{0001} is a better choice. In the thermal decomposition of SiC{0001}, wafer-scale graphene with a controlled number of layers can be grown spontaneously on the semi-insulating SiC substrate. In this review article, we describe the features of epitaxial graphene grown by thermal decomposition of SiC{0001} surfaces, particularly focusing on its growth mechanisms.

2. Growth of graphene by thermal decomposition of SiC

Figure 1 is a high-resolution transmission electron microscope (HRTEM) image of monolayer graphene epitaxially grown on SiC(0001). Graphene can be observed as a dark line contrast under the Scherzer focus condition at the accelerating voltage of 200 kV. The basic process of the thermal decomposition of SiC is shown in figure 2. Due to the difference in the vapor pressures, silicon atoms easily sublime from the surface in a vacuum at a high temperature compared to carbon atoms, and then the remaining carbon atoms form graphene. The graphitization phenomenon induced by thermal decomposition of SiC(0001) was already known in 1965 [27]. Early x-ray diffraction studies revealed the crystallographic orientation relation between graphene and SiC [27, 28]. In 1998, it was found that graphene grew via the $6\sqrt{3}\times6\sqrt{3}$R30 reconstructed surface [29]. Few-layer graphene (FLG) on SiC{0001} was first witnessed directly by HRTEM observation in 2000 [30]. In 2004, which is the same year when Novoselov *et al* reported the Dirac nature of exfoliated graphene, Berger *et al* also revealed the 2DEG properties of epitaxial graphene on SiC [31, 32]. This discovery attracted a great deal of attention because this material is compatible with current silicon-based semiconductor technology.

One advantage of graphene on SiC{0001} is that graphene can be grown directly on the semi-insulating substrate. In other words, we can fabricate graphene field-effect transistor devices over the entire wafer. Using epitaxial graphene on SiC(0001), the high carrier mobility of several 10^4 cm^2 Vs^{-1} was achieved by the optimization of the carrier concentration [33, 34]. An analogue radio frequency transistor using graphene on SiC had a 300 GHz cutoff-frequency and 70 GHz oscillation-frequency, and an integrated circuit using epitaxial graphene was realized [22, 23, 35, 36]. Despite the high cost of the SiC single crystal, these outstanding properties are still attractive. Thus, high-frequency transistors based on epitaxial graphene on SiC may well find applications within a decade [24].

Recent research on epitaxial graphene is supported by progress in the growth of SiC single crystal. In particular, the density of dislocations appearing on the SiC surface has significantly decreased in the last decade. The surface treatment technology has also been highly developed. This progress has increased the quality of graphene grown on SiC.

The SiC surfaces on which graphene can be grown include the Si-terminated (0001) and the C-terminated (000$\bar{1}$) faces. The structure of these faces is shown in figure 3. The SiC crystal structure is characterized by the stacking of the SiC bilayer. One side of the bilayer is Si-terminated, and the other side is C-terminated. The distinctive features of graphene grown on them are notably different. The most characteristic

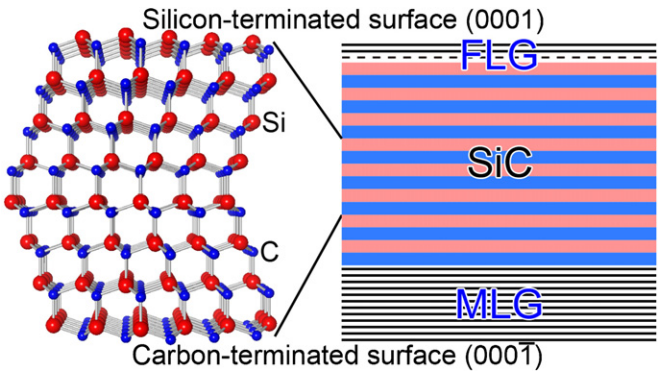

Figure 3. Crystal structure of hexagonal SiC and its Si-terminated (0001) and C-terminated (000$\bar{1}$) surfaces. Eight SiC bilayers are shown. On the Si-face, FLG with a buffer layer can be homogeneously grown, and on the C-face, MLG can be grown.

feature of graphene on the Si-face is the presence of a buffer layer, as indicated by the broken lines in figures 1, 2 and 3 [37, 38]. Mainly due to the buffer layer, graphene on the Si-face has *n*-type conduction, and the mobility is lower than that on the C-face [39, 40]. This buffer layer can be turned into monolayer graphene by hydrogen intercalation into the interface between the buffer layer and SiC [41]. This is called the 'quasi-freestanding monolayer graphene'. By the hydrogen intercalation, the carrier mobility can be improved and the carrier type can be changed from *n*-type to *p*-type [42]. On the Si-face, homogeneous monolayer, bilayer, and further layers can be grown [43, 44]. Figure 4 shows the HRTEM images of monolayer, bilayer, trilayer and eight layers of graphene [37]. Early angle-resolved photoelectron spectroscopy (ARPES) study revealed that the bilayer graphene exhibited the electronic structure of AB-stacking (Bernal stacking), and that the trilayer had the mixed stackings of ABA and ABC (rhombohedral stacking) [45]. The stacking sequence of more than three layers was directly observed by the HRTEM, and it was revealed that they exclusively exhibited the ABC-stacking [46]. Recent ARPES measurement showed that the homogeneous quasi-freestanding trilayer graphene had the ABC-stacking [47]. It is then suggested that multilayer graphene (MLG) has some effect to stabilize the ABC-stacking due to the SiC substrate, which is less stable in bulk graphite.

On the other hand, graphene on the C-face typically grows in a multilayer form. MLG on this face is rotationally stacked, has no buffer layer, and is less homogeneous [48, 49]. At the same carrier density, the carrier mobility of graphene on the C-face is higher than that on the Si-face [40]. We then have two approaches for device applications. One is that we improve the mobility using homogeneous large-area graphene grown on the Si-face. The other is that we upgrade the quality using high mobility graphene grown on the C-face. For both approaches, we need to understand the growth mechanisms. The difference in the structure and properties of graphene on the Si- and C-face suggests that there are differences in the growth mechanisms. In the following sections, we describe the details of the growth mechanisms revealed experimentally and theoretically.

3. Graphene growth mechanism: experimental results

We first describe the graphene growth mechanism on the Si-face. In the last century, the surface changes on the Si-face were investigated by x-ray and low-energy electron diffraction studies [27–29]. According to them, when annealed under vacuum at about 1050 °C, the SiC surface first changes to exhibit a $\sqrt{3}\times\sqrt{3}$R30 reconstruction, which is characterized by the presence of Si adatoms on top of the clean Si-terminated surface [50]. It then turns into a $6\sqrt{3}\times6\sqrt{3}$R30 reconstruction by further heating at 1100 °C. This reconstructed surface has a honeycomb lattice consisting solely of carbon atoms, but this layer has a strong interaction with the SiC substrate. A graphite multilayer grows on top of this surface at higher temperatures.

Even though the graphene growth process on the Si-face detailed above is well understood, we should clarify the identity of the nucleation site and the growth direction for obtaining high-quality graphene. In particular, we focus on the role of the steps on the surface. Figure 5 shows some typical HRTEM images of graphene, corresponding to the nucleation and the growth stages [51]. In this case, graphene was grown on the 6H-SiC(0001) substrate, and the surface was pre-treated

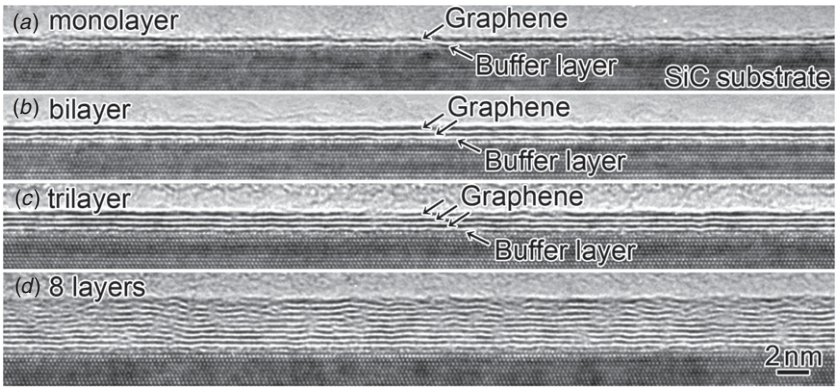

Figure 4. HRTEM images of (*a*) monolayer, (*b*) bilayer, (*c*) trilayer and (*d*) eight-layer graphene grown on the Si-face at different temperatures. Reproduced with permission from [37]. © 2009 Elsevier.

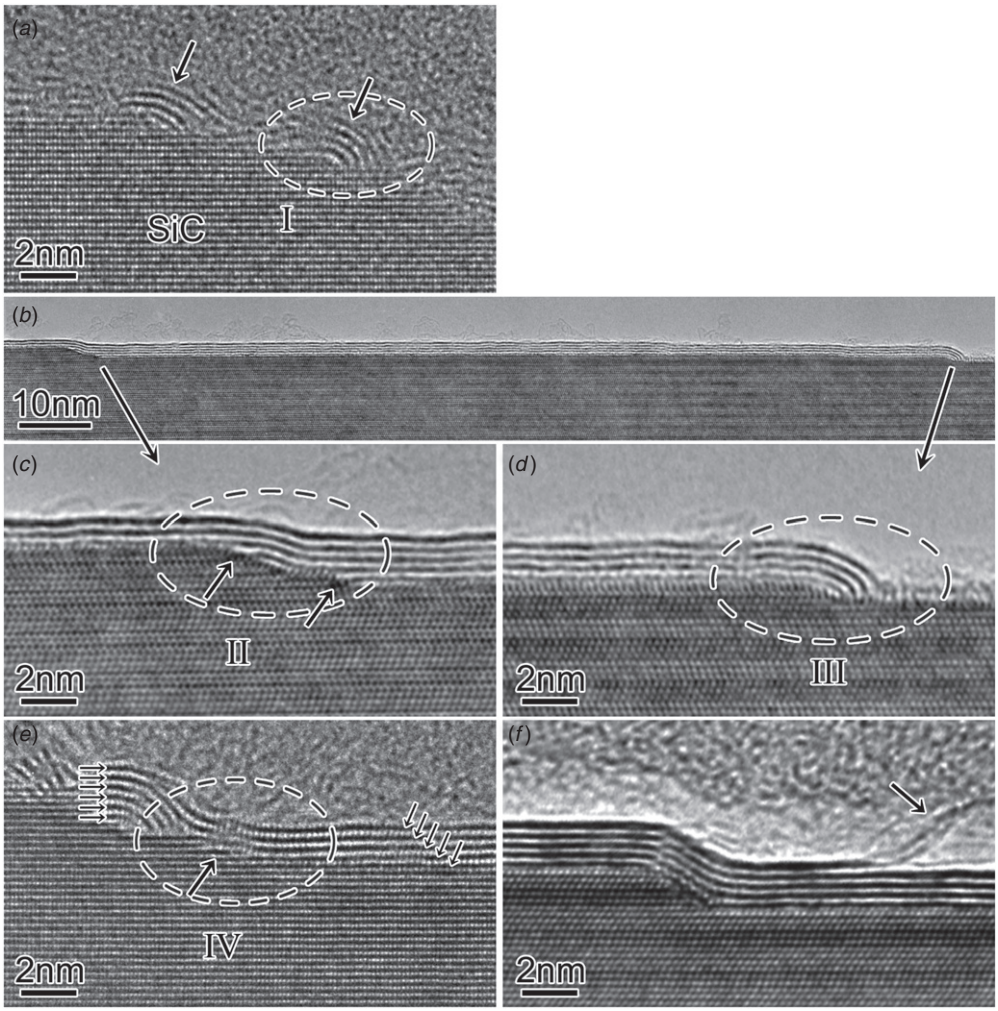

Figure 5. HRTEM images of graphene on the Si-face showing the nucleation and growth process. (*a*) Initial growth at steps. (*b*) Wide-area scan at a later stage of growth. The images in (*c*) and (*d*) are enlargements of parts of (*b*). Images (*e*) and (*f*) show graphene around the step. Reproduced with permission from [51]. © 2010 Elsevier.

by the chemical mechanical polishing to completely remove scratches and obtain the flat step-terrace structure. We used both the on-axis and 4°-off 6H-SiC substrates in order to clarify the role of the steps. Graphitization was carried out in a high vacuum at different temperatures. More details about the procedure were described in our previous papers [37, 38, 46, 51]. Monolayer and bilayer graphene were grown at 1300 and 1400 °C, which will be described again. In the image in (*a*), four curved graphene layers cover the SiC steps. This indicates that graphene was initially formed around the steps. Another interesting feature in (*a*) is that the edges of the graphene nucleus terminate almost perpendicularly on the lower terrace. The wide-area image in (*b*) indicates that graphene growth proceeds from the right steps to the left terrace region. The images in (*c*) and (*d*) are enlargements of parts of (*b*). In (*d*), curved graphene layers on a SiC step spread over the terrace region to the left. This curved graphene also terminates on the lower terrace standing vertically. In another step-like region in (*c*), there are five and three layers on the right and left sides, respectively. Here, graphene layers seemed to grow from the right to the left. In other words, the growth of the two layers stopped in this region. In (*e*), the arrow indicates three poorly resolved graphene layers on a step. On the right side of the step, five layers are clearly observed, while on the left side, there are six layers. These results can be understood as a coalescence of the graphene layers. In the image (*f*), five graphene layers appear to continuously cover the SiC step.

The proposed growth mechanism is summarized in figure 6. First, silicon atoms at the step position are preferentially sublimed (*a*). This is because the silicon atoms at the step-edge have more dangling bonds and so have weaker bonds than those in the bulk and on the terrace. Consequently, the remaining carbon atoms aggregate and form curved graphene layers covering the step (*b*). This suggests that the step acts as a carbon trapping site. In fact, a few layers were often observed at the step. The graphene nucleated around the step then grew over the terrace region above the step (*c*). The next graphene layer is then formed beneath the first layer at the step and grows in the same direction as the first layer. The growth is occasionally pinned by a surface defect, as shown in the circle in (*d*). Graphene grows also on the lower terrace (*d*), eventually resulting in the coalescence (*e*). The graphene layers covering the steps are finally formed by repetitions of the above layer-by-layer phenomena (*f*) and (*g*).

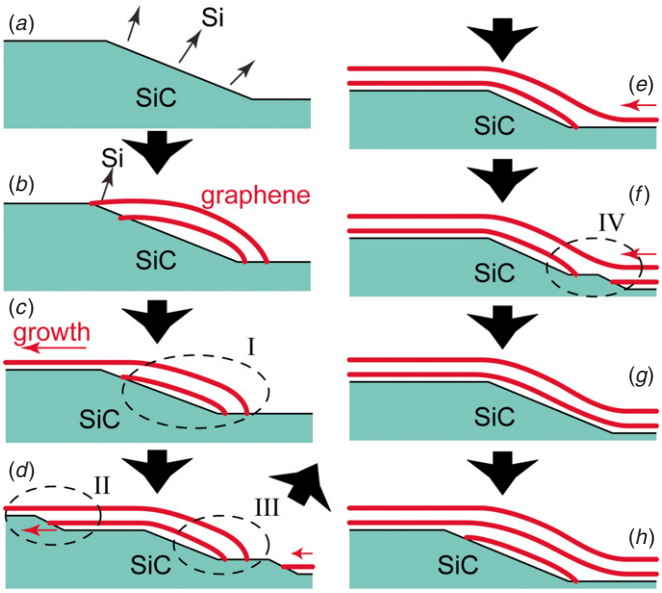

Figure 6. Schematic diagram of the growth mechanism of graphene on the Si-face. Circles with broken lines correspond to the regions in figure 5. Reproduced with permission from [51]. © 2010 Elsevier.

In more detail, graphene grew only on the upper terrace after the nucleation. The origin is as follows. Curved graphene nucleated around the step always terminates on the lower terrace as shown in figures 5(*a*) and (*d*). Accordingly, terrace decomposition should have been required in order to grow graphene towards the lower terrace. However, terrace decomposition clearly needs a higher energy than step decomposition does. In other words, the upper terrace decomposition together with a retreating step, as in figure 5(*d*), is much preferred over the decomposition of the lower terrace. This idea is supported by figure 7 [52]. In the HRTEM image in (*a*), no graphene is present in the center. Trilayer graphene spreads to the upper terraces from the steps on both sides of the middle base region. Trilayer graphene requires the decomposition of about nine SiC bilayers with respect to the number of carbon atoms. This fact suggests that this region should have been a basin over nine SiC bilayers deep before decomposition as shown in (*b*). In the image in (*a*), trilayer graphene terminates on the lower terraces which correspond to the bottom of the basin, while no graphene was found there. Thus, this image clearly indicates that graphene nucleated at the step always grows on the upper terrace, not on the lower terrace as shown in (*c*). The AFM topography (*d*) and phase (*e*) images also support this mechanism. In the phase image, a larger layer number of graphene has a brighter contrast than less-layered graphene due to its hardness and the difference in adhesion [52]. In (*e*), bright and dark regions correspond to the trilayer and bilayer, respectively. It should be noted here that there is a larger trilayer area on the left side (upper terrace) of the step denoted by the red broken line than that on the right side (lower terrace). These results lead to the conclusion that graphene on the Si-face that nucleated at the step grows over almost all the upper terrace shown by the blue arrows. Based on this growth mechanism, homogeneous monolayer

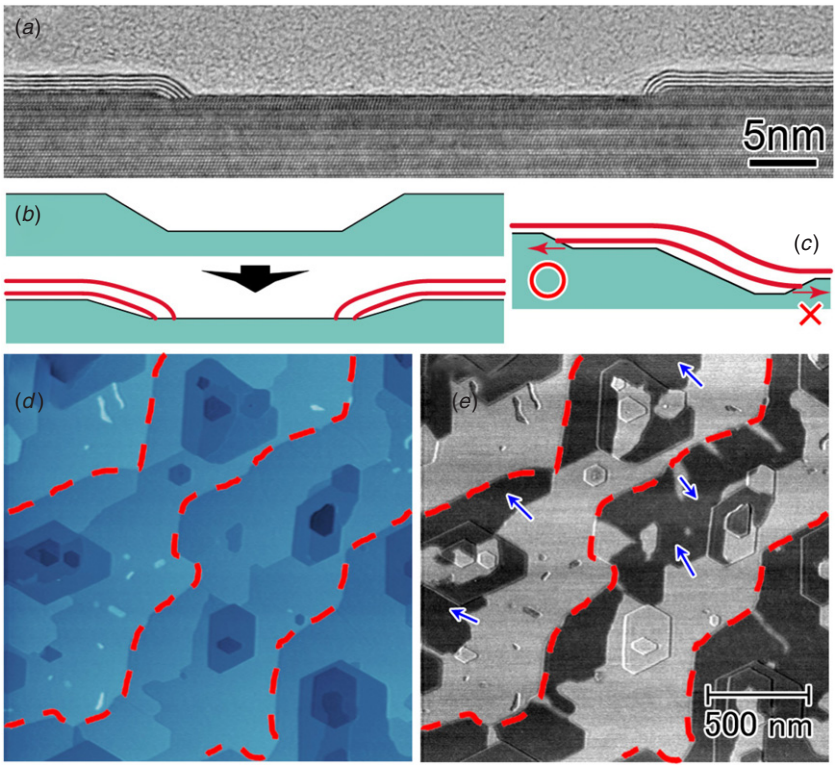

Figure 7. HRTEM and AFM images showing the graphene growth direction. (*a*) and (*b*) Graphene formed around a pit on the Si-face. Graphene nucleates at the step, terminates on the lower terrace, and then grows to the upper terrace as shown in (*c*). (*d*) and (*e*) The AFM topography and phase images of the same area. The topographic image is shown with a height scale of 6 nm. In the phase image, bright and dark areas correspond to the trilayer and bilayer regions, respectively. Reproduced with permission from [52]. © 2013 IOP Publishing.

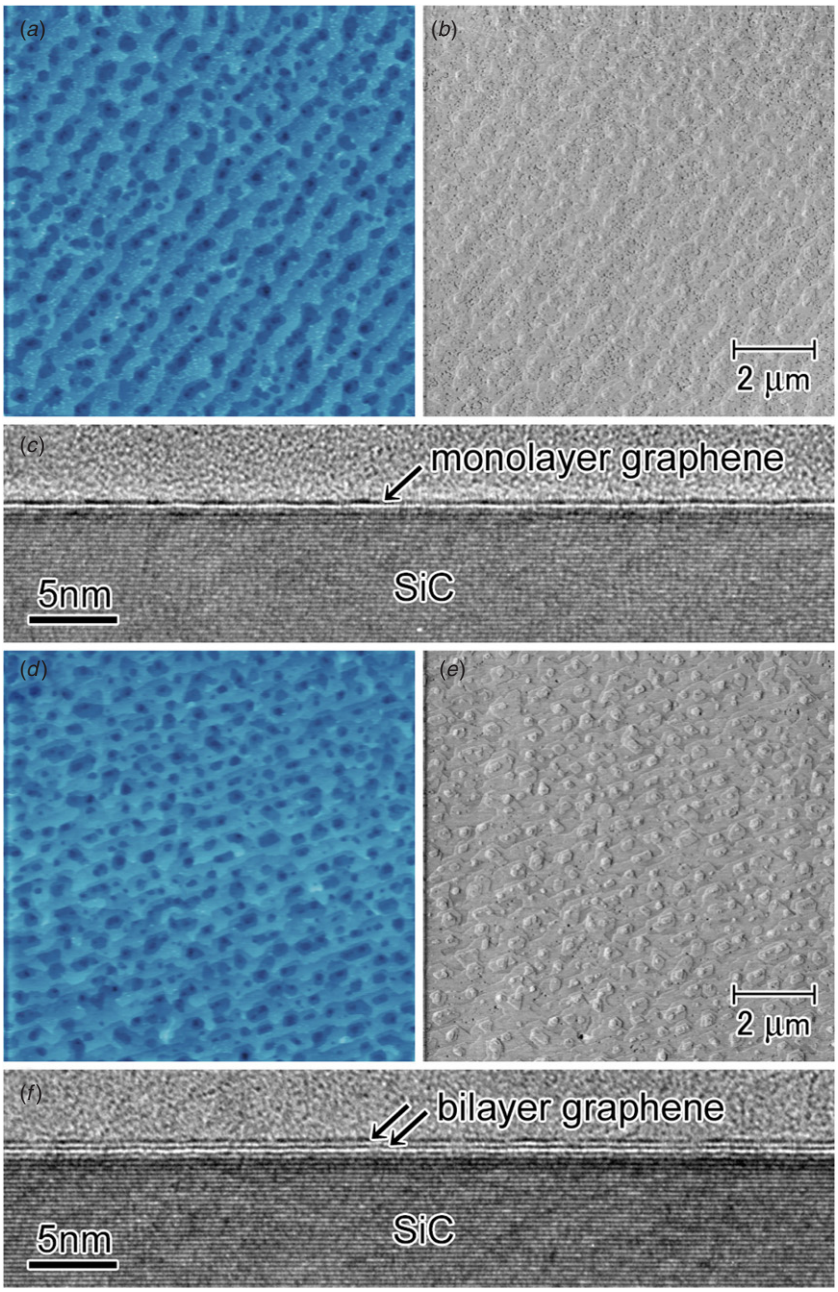

Figure 8. Wide-area AFM and TEM images of (*a*) and (*b*), (*c*) monolayer, and (*d*)–(*f*) bilayer graphene. (*a*) and (*d*) The topography images, and (*b*) and (*e*) are the phase images. The height scale in (*a*) and (*d*) is 6 nm. The typical step heights in (*a*) and (*d*) are 0.50 and 0.75 nm. R_a and R_{ms} values are (*a*) $R_a = 0.40$ nm, $R_{ms} = 0.51$ nm, (*d*) $R_a = 0.33$ nm, $R_{ms} = 0.43$ nm. Reproduced with permission from [52]. © 2013 IOP Publishing.

and bilayer graphene growth can now be possible as shown in figure 8 [52]. Monolayer and bilayer graphene was grown at 1300 and 1400 °C. Higher magnification AFM phase images show the surface coverage of graphene [52]. The monolayer coverage 1300 °C sample was 84%, and the other area was SiC or buffer layer. Bilayer was 99% (almost all area). In the area of HRTEM images we observed, only homogeneous monolayer or bilayer was observed, indicating the high coverage.

On the C-face, graphene typically grows in a multilayer form. This suggests that the C-face is much more highly reactive than the Si-face. To obtain high-quality and homogeneous FLG growth on the C-face, reducing the reactivity is important. In order to reduce the reactivity and suppress Si sublimation, graphitization in an Ar atmosphere is effective [53, 54]. Increasing the Ar pressure during graphene growth suppresses the decomposition, leading to more homogeneous graphene layers. We found that homogeneous graphene growth on the C-face was possible in 6 atm Ar [54].

Figure 9 shows the HRTEM images of graphene annealed at different temperatures on the C-face. First, by annealing at (*a*) 1350 °C for 1 h, we find a very flat SiC surface with no graphene. Figure 9(*b*) shows the surface annealed at 1350 °C for 6 h. As shown by two arrows, five or six curved graphene layers are formed covering the crater with a width of 2–4 nm

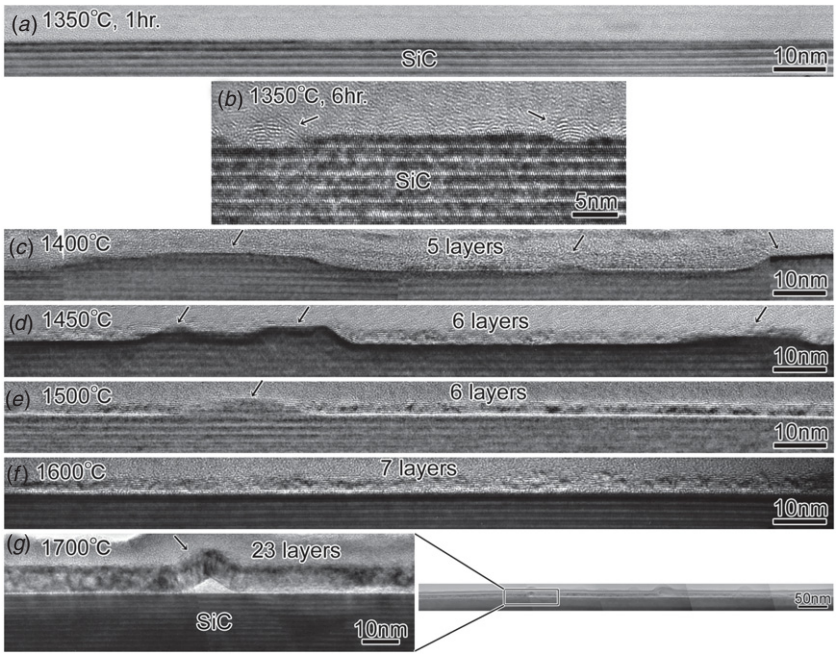

Figure 9. HRTEM images of graphene grown on the C-face at (*a*) and (*b*) 1350, (*c*) 1400, (*d*) 1450, (*e*) 1500, (*f*) 1600 and (*g*) 1700 °C in 6 atm Ar. In (*a*) and (*b*), the annealing time is 60 and 360 min, respectively. In (*g*), a low-magnification image is also shown. Reproduced with permission from [54]. © 2011 American Physical Society.

and a depth of 1–1.5 nm. In other regions in (*b*), graphene with clear contrast was not observed. These results suggest that graphene nuclei of several layers thickness were first generated in the craters. After annealing at 1400 °C in (*c*), some wide knolls, as shown by arrows, can be seen. In this image, five graphene layers are observed in the crater region, while there are very few layers on the knoll. After annealing at (*d*) 1450 °C and (*e*) 1500 °C, similar rough surfaces were observed and the number of graphene layers was about six in the crater and zero to two on the knoll with a width of 10–20 nm. The most striking feature in these images is that the area of the crater where graphene was present increased with an increase in the temperature. After annealing at 1600 °C, shown in (*f*), no knolls could be observed any more, and seven graphene layers had grown over the whole surface. Interestingly, the number of graphene layers hardly changes with increasing temperature below 1600 °C. However, at 1700 °C, 23 graphene layers cover the SiC surface and wrinkles are observed.

We propose the growth mechanism of graphene on the C-face, shown in figure 10. At a low temperature, Si atoms in the local area sublime, making small craters on the surface. Although we could not define the nucleation sites, surface defects, such as atomic steps and screw dislocations play important roles as the starting point of decomposition. A graphene nucleus is formed covering the craters as shown in figures 9(*b*) and 10(*b*). Nucleated graphene typically contains three to six layers. After the nucleation, Si atoms at the edge of the crater sublime, leading to the lateral growth shown in (*c*) and (*d*). At these stages, zero or very few graphene layers are created on the knoll, suggesting that the carbon source is not the knoll but the edge of the crater. The area of the knoll with respect to the crater decreases with the amount of graphene growth. Finally, graphene layers cover the whole

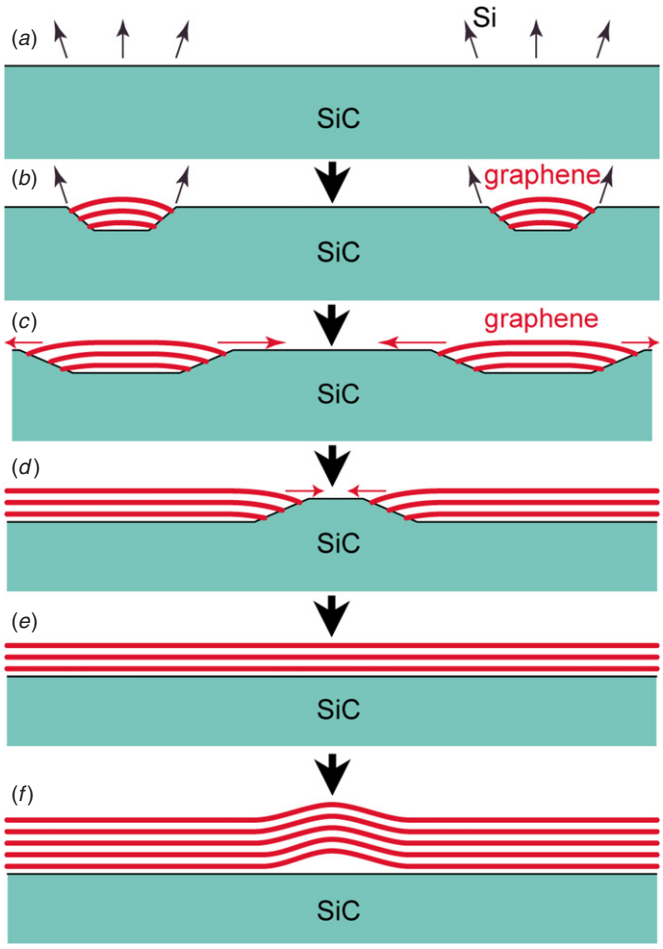

Figure 10. Proposed growth mechanism of graphene on the C-face. Reproduced with permission from [54]. © 2011 American Physical Society.

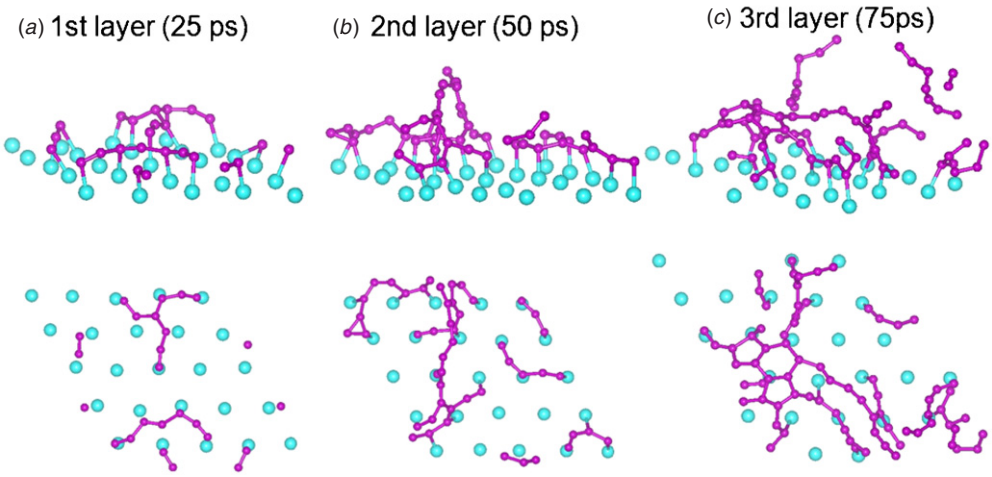

Figure 11. DFTB simulation results of the Si-face terrace model at 2000 K. The upper and lower parts are side- and top-views. Snapshots after (*a*) the first, (*b*) the second and (*c*) the third SiC bilayer were decomposed, corresponding to the presence of 25, 50 and 75 free carbon atoms, respectively, are shown. Reproduced with permission from [63]. © 2013 AIP Publishing.

surface as shown in (*e*) via the disappearance of the small knoll shown in (*d*). After a complete graphene film is obtained, decomposition occurs in the normal direction and the number of layers increases at this stage, together with the wrinkling phenomena (*f*). In this mechanism, the number of graphene layers does not change until graphene covers the surface. This suggests that for the control of the number of layers, the amount of decomposition at the nucleation stage should be properly controlled.

The difference in the graphene growth mechanisms on the Si- and C-face may originate from the difference in the reactivity of these faces. According to the previous reports, the C-face is more reactive than the Si-face with respect to oxidation and epitaxial SiC growth [55, 56]. We then suppose that decomposition of SiC on the C-face is faster than that on the Si-face. On the highly reactive C-face, local decomposition occurs at various sites on the surface, leading to the formation of graphene in the crater [54]. The presence of screw dislocations and atomic steps plays a prominent role at the nucleation sites. In contrast, on the Si-face, graphene nucleates only at the locally reactive step edges instead of on the terrace.

4. Graphene growth mechanism: theoretical results

The above mentioned experimental results were obtained using samples annealed in advance. In other words, the atomic scale behavior of the carbon atoms after silicon removal at high temperature has not yet been clarified. This is because the graphene growth phenomena take place at high temperature of more than 1200 °C, which makes atomic scale experimental investigations extremely difficult. Accordingly, we then focused on molecular dynamics simulation.

Theoretical reports about graphene growth on SiC have been published by several groups. Tang and co-workers performed molecular dynamics simulation of the structural changes at several finite temperatures when sufficient carbon atoms for monolayer formation were added at one time [57]. Kageshima and co-workers reported density functional calculation results of the most stable ground-state structure when the carbon atoms were adsorbed one-by-one on the SiC(0001) surface [58, 59]. Ming and Zangwill carried out modeling and simulation of graphene growth on the SiC(0001) stepped surface by the Monte-Carlo method [60, 61]. Inoue and co-workers reported density functional calculation of the carbon network expansion in the buffer layer by adsorbing carbon atoms one-by-one at 0 K [62]. In other words, an atomic-scale graphene growth simulation following a one-by-one removal of Si atoms at a finite temperature has never been reported. We show here our results about the behavior of the carbon atoms after the silicon atoms were removed one-by-one using highly accurate density-functional tight-binding (DFTB) simulations [63].

In order to reproduce the graphene growth process, we adopted three initial models; the terrace model, the step model and the step-growth model. In the terrace model, we used a $5 \times 5 \times 0.5$ unit cell of 6H-SiC (0001) Si-face together with periodic boundary conditions only in the *x* and *y* directions. We first set the desired temperature and equilibrated the structure, and then removed the silicon atoms one-by-one at intervals of 1 ps in order to mimic the decomposition process. After the first SiC bilayer was decomposed (25 Si atoms were removed), the second bilayer starts to be decomposed. We need three-bilayer decomposition to obtain enough carbon atoms for graphene, because in one bilayer there is about 1/3 of the atom concentration needed for a graphene monolayer. In the step model, we assumed a step with a three SiC bilayer height (0.75 nm), pointing toward the $[11\bar{2}0]$ direction. In the step-growth model, we placed curved graphene in advance, and then start the decomposition.

Figure 11 shows snapshots after (*a*) one, (*b*) two and (*c*) three SiC bilayers were decomposed at 2000 K. We simulated five trajectories for 1500 and 2000 K, and found similar results. In the supplementary material in our previous paper, the movie result of another trajectory is shown [63]. As we can see in figure 11(*a*), the carbon atomic chains dispersed on the surface after one bilayer has decomposed. We can also recognize that after the silicon removal, the remaining carbon atoms formed

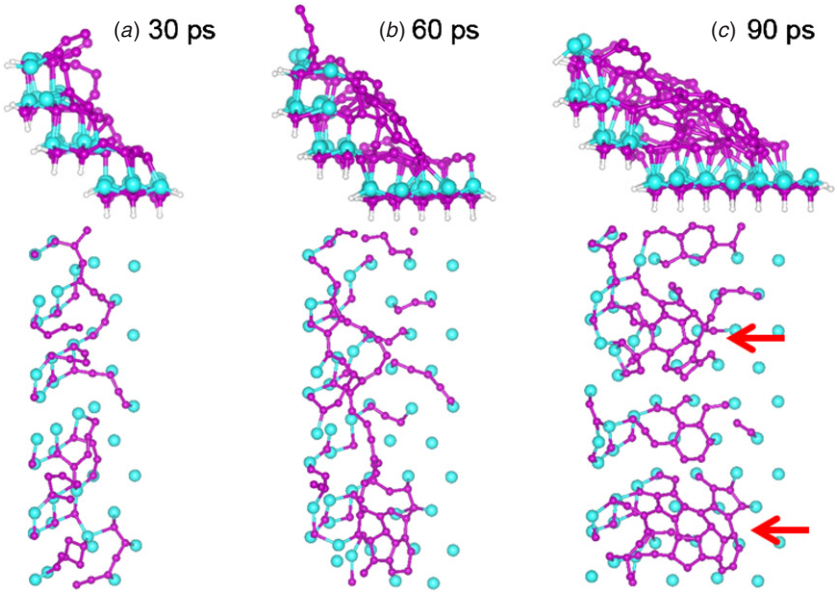

Figure 12. DFTB simulation results of the Si-face step model at 2000 K. Snapshots after the removal of (*a*) 30, (*b*) 60 and (*c*) 90 silicon atoms are shown. The upper and lower parts are side- and top-views. Reproduced with permission from [63]. © 2013 AIP Publishing.

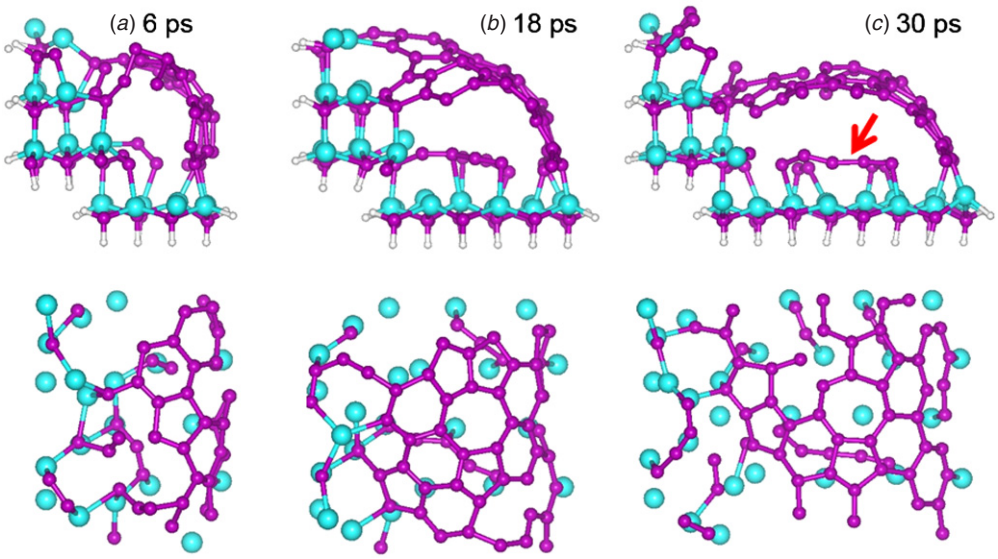

Figure 13. DFTB simulation results of the step-growth model at 2000 K, showing the growth process and second layer nucleation. Snapshots after the removal of (*a*) 30, (*b*) 60 and (*c*) 90 silicon atoms are shown. Reproduced with permission from [63]. © 2013 AIP Publishing.

a horizontal bond. However, after the decomposition of two bilayers, the carbon chains became longer, and a portion of the chains desorbed. When we carefully examined the movie, we realize that the second layer decomposition corresponds to the loss of the foothold for the free carbon atoms, resulting in the desorption. Finally, after three bilayers had decomposed, the long carbon chains formed a three-dimensional network and some chains desorbed, although a few five- and six-membered rings can be observed. These results suggest that it is difficult to grow perfect graphene by the decomposition of a flat terrace.

Figure 12 shows the results of the step model. In figure 12(*a*), where 30 silicon atoms were removed and the same number of carbon atoms became free, we see that many carbon chains were formed and they were connected with each other. Carbon chains that are not contacting the substrate are rarely found. There was a chain sticking upward in (*b*), but it finally turned back towards the surface in (*c*). Carbon networks consisting of five- and six-membered rings were formed in (*b*). Several such networks were observed, their size increased, and they were connecting with the retreating step as shown by the arrows in (*c*). Although the carbon network formed in this way does not yet possess the complete graphene honeycomb structure, we think that further simulation would lead to the ideal graphene formation. These differences between the terrace and step models suggest that the surface silicon atoms at the step-edge having many dangling bonds can act as carbon-trapping sites, which is consistent with the experimental results shown in figure 5.

In figure 13, the snapshots of the step-growth model are shown. After (*a*) 6 and (*b*) 18 ps, the carbon network containing the five-, six- and seven-membered rings expanded. After (*c*) 30 ps, in addition to the expansion, the second layer core (chain) nucleated beneath the first layer, as indicated by an arrow. We can see in the movie that the released carbon atoms at the top step-edge easily connected with the right-side network. We can also find the robustness of the edge of graphene. In all snapshots in figure 13, the lower left edge of the sheet was strongly bonded to the substrate. This suggests that once the edge terminates on a terrace, it is fixed in place and does not grow further even at 2000 K.

Thus, we conclude that a graphene network easily nucleates at a step on the SiC surface, due to the trapping effect of the silicon atoms at the step-edge. After nucleation, graphene can grow by further decomposition and subsequent step retreat. These simulation results and experimental results in the previous section are in excellent agreement with each other.

5. Conclusions and prospects for graphene on SiC

The simplest monatomic layer, graphene, can be obtained by the thermal decomposition of SiC, and its growth mechanisms were reviewed. By using this technique, homogeneous graphene with a controlled number of layers can be grown spontaneously on the semi-insulating substrate. On the Si-face, graphene nucleates at steps, and then grows over the terraces in a layer-by-layer fashion. On the C-face, it nucleates not only at steps, but also on the terraces, and then it grows in all directions on the surface.

Graphene on SiC is suited for use in high-frequency transistor applications [35, 36]. In addition, because we can use high-quality single crystal SiC, it can also be a platform for various types of graphene. Forming a graphene nanoribbon is a promising technique to introduce a bandgap into graphene, and a high-quality graphene nanoribbon array on SiC can be grown in several ways [64–67]. Simultaneous growth of graphene and an electrode is possible using a TiC thin film grown on SiC, and boron-doped graphene can be grown using a B_4C/SiC substrate [68, 69]. Further progress in this area will open a new field in the science and technology of semiconducting layer materials.

Acknowledgments

This work was partially supported by the Asahi Glass Foundation and JSPS Grant-in-Aid for Scientific Research on Innovative Areas 'Science of Atomic Layers'.

References

[1] Bernal J D 1924 *Proc. R. Soc. Lond. A* **106** 749
[2] Wallace P R 1947 *Phys. Rev.* **71** 622
[3] Matsubara K, Sugihara K and Tsuzuku T 1990 *Phys. Rev.* B **41** 969
[4] Slack G A 1962 *Phys. Rev.* **127** 694
[5] Satterthwaite C B and Ure R W 1957 *Phys. Rev.* **108** 1164
[6] Semiletov S A 1956 *Kristallografiya* **1** 403
[7] Rowe D M 1995 *Handbook of Thermoelectrics* (Boca Raton, FL: CRC Press)
[8] Wan C, Wang Y, Wang N, Norimatsu W, Kusunoki M and Koumoto K 2010 *Sci. Technol. Adv. Mater.* **11** 044306
[9] Wan C, Wang Y, Wang N, Norimatsu W, Kusunoki M and Koumoto K 2011 *J. Electron. Mater.* **40** 1271
[10] Wan C, Wang Y, Norimatsu W, Kusunoki M and Koumoto K 2012 *Appl. Phys. Lett.* **100** 101913
[11] Bednorz J G and Muller K A 1986 *Z. Phys.* B **64** 189
[12] Bednorz J G and Muller K A 1988 *Rev. Mod. Phys.* **60** 585
[13] Imada M, Fujimori A and Tokura Y 1998 *Rev. Mod. Phys.* **70** 1039
[14] Norimatsu W and Koyama Y 2006 *Phys. Rev.* B **74** 085113
[15] Norimatsu W and Koyama Y 2007 *Phys. Rev.* B **75** 104416
[16] Norimatsu W and Koyama Y 2007 *Phys. Rev.* B **75** 235121
[17] Novoselov K S, Geim A K, Morozov S V, Jiang D, Zhang Y, Dubonos S V, Grigorieva I V and Firsov A A 2004 *Science* **306** 666
[18] Novoselov K S, Geim A K, Morozov S V, Jiang D, Katsnelson M I, Grigorieva I V, Dubonos S V and Firsov A A 2005 *Nature (Lond.)* **438** 197
[19] Nair P R, Blake P, Grigorenko A N, Novoselov K S, Booth T J, Stauber T, Peres N M R and Geim A K 2008 *Science* **320** 1308
[20] Dean C R *et al* 2010 *Nature Nanotechnol.* **5** 1
[21] Mayorov A S *et al* 2011 *Nano Lett.* **11** 2396
[22] Lin Y-M, Dimitrakopoulos C, Jenkins K A, Farmer D B, Chiu H-Y, Grill A and Avouris P H 2010 *Science* **327** 662
[23] Lin Y-M *et al* 2011 *Science* **332** 1294
[24] Novoselov K S, Fal'ko V I, Colombo L, Gellert P R, Schwab M G and Kim K 2012 *Nature (Lond.)* **490** 192
[25] Eizenberg M and Blakely J M 1979 *Surf. Sci.* **82** 228
[26] Li X *et al* 2009 *Science* **324** 1312
[27] Badami D V 1965 *Carbon* **3** 53
[28] van Bommel A J, Crombeen J E and van Tooren A 1975 *Surf. Sci.* **48** 463
[29] Forbeaux I, Themlin J-M and Debever J-M 1998 *Phys. Rev.* B **58** 16396
[30] Kusunoki M, Suzuki T, Hirayama T, Shibata N and Kaneko K 2000 *Appl. Phys. Lett.* **77** 531
[31] Berger C *et al* 2004 *J. Phys. Chem.* B **108** 19912
[32] Berger C *et al* 2006 *Science* **312** 1191
[33] Jobst J, Waldmann D, Speck F, Hirner R, Maude D K, Seyller T H and Weber H B 2010 *Phys. Rev.* B **81** 195434
[34] Tanabe S, Sekine Y, Kageshima H, Nagase M and Hibino H 2011 *Phys. Rev.* B **84** 115458
[35] Avouris P and Xia F 2012 *MRS Bulletin* **37** 1225
[36] Guo Z *et al* 2013 *Nano Lett.* **13** 942
[37] Norimatsu W and Kusunoki M 2009 *Chem. Phys. Lett.* **468** 52
[38] Norimatsu W and Kusunoki M 2010 *J. Nanosci. Nanotechnol.* **10** 3884
[39] Ristein J, Mammadov S and Seyller T H 2012 *Phys. Rev. Lett.* **108** 246104
[40] Tedesco J L *et al* 2009 *Appl. Phys. Lett.* **95** 122102
[41] Riedl C, Colleti C, Iwasaki T, Zakharov A A and Starke U 2009 *Phys. Rev. Lett.* **103** 246804
[42] Robinson J A, Hollander M, LaBella M III, Trumbull K A, Cavalero R and Snyder D W 2011 *Nano Lett.* **11** 3875
[43] Virojanadara C, Syvajarvi M, Yakimova R, Johansson L I, Zakharov A A and Balasubramanian T 2008 *Phys. Rev.* B **78** 245403
[44] Emtsev K V *et al* 2009 *Nature Mater.* **8** 203
[45] Ohta T, Bostwick A, McChesnery J L, Seyller T H, Horn K and Rotenberg E 2007 *Phys. Rev. Lett.* **99** 206802
[46] Norimatsu W and Kusunoki M 2010 *Phys. Rev.* B **81** 161410(R)
[47] Colletti C *et al* 2013 *Phys. Rev.* B **88** 155439

[48] Hass J, Varcho F, Millan-Otoya J E, Sprinkle M, Sharma N, de Heer W A, Berger C, First P N, Magaud L and Conrad E H 2008 *Phys. Rev. Lett.* **100** 125504
[49] Kuroki J, Norimatsu W and Kusunoki M 2012 *e-J. Surf. Sci. Nanotechnol.* **10** 396
[50] Starke U, Schardt J, Bernhardt J, Franke M and Heinz K 1999 *Phys. Rev. Lett.* **82** 2107
[51] Norimatsu W and Kusunoki M 2010 *Physica E* **42** 691
[52] Norimatsu W and Kusunoki M 2014 *J. Phys. D: Appl. Phys.* **47** 094017
[53] Tedesco J L *et al* 2010 *Appl. Phys. Lett.* **96** 222103
[54] Norimatsu W, Takada J and Kusunoki M 2011 *Phys. Rev.* B **84** 035424
[55] Matsunami H and Kimoto T 1997 *Mater. Sci. Eng. R* **20** 125
[56] Ray E A, Rozen J, Dhar S, Feldman L C and Williams J R 2008 *J. Appl. Phys.* **103** 023522
[57] Tang C, Meng L, Xiao H and Zhong J 2008 *J. Appl. Phys.* **103** 063505
[58] Kageshima H, Hibino H, Nagase M and Yamaguchi H 2009 *Appl. Phys. Express* **2** 065502
[59] Kageshima H, Hibino H, Yamaguchi H and Nagase M 2011 *Japan. J. Appl. Phys.* **50** 095601
[60] Ming F and Zangwill A 2011 *Phys. Rev.* B **84** 115459
[61] Ming F and Zangwill A 2012 *J. Phys. D: Appl. Phys.* **45** 154007
[62] Inoue M, Kageshima H, Kangawa Y and Kakimoto K 2012 *Phys. Rev.* B **86** 085417
[63] Morita M, Norimatsu W, Qian H-J, Irle S and Kusunoki M 2013 *Appl. Phys. Lett.* **103** 141602
[64] Liu G *et al* 2012 *ACS Nano* **6** 6786
[65] Kajiwara T, Nakamori Y, Visikovskiy A, Iimori T, Komori F, Nakatsuji K, Mase K and Tanaka S 2013 *Phys. Rev.* B **87** 121407(R)
[66] Baringhaus J *et al* 2014 *Nature* **506** 349–54
[67] Baringhaus J, Edler F and Tegenkamp C 2013 *J. Phys.: Condens. Matter* **25** 392001
[68] Norimatsu W, Hirata K, Yamamoto Y, Arai S and Kusunoki M 2012 *J. Phys.: Condens. Matter* **24** 314207
[69] Kimura K, Shoji K, Yamamoto Y, Norimatsu W and Kusunoki M 2013 *Phys. Rev.* B **87** 075431